

Radial Force Control of a Switched Reluctance Motor with Two-Phase Sinusoidal Excitations

Feng-Chieh Lin

Sheng-Ming Yang

Department of Mechanical and Electro-mechanical Engineering
Tamkang University, Tamsui
Taipei County, Taiwan

Abstract - Due to its special structure, the shaft radial force and torque of switched reluctance motor can be separately controlled by proper selection of pole currents. When all the pole currents are controlled independently, it is possible to produce the required radial force to cancel the existing radial force caused by non-uniform air gap or external load, and consequently motor vibrations can be reduced. In this paper, a radial force control scheme which use single or two phase sinusoidal excitations for 12/8 pole SRM is proposed. The pole currents of the conduction phase are energized with phase-shifted sinusoidal currents. Depending on the requested radial force and motor torque, the phase with descending-inductance may also be energized to increase radial force production. The requested force and torque are synthesized from the force and torque produced by these phases. The proposed scheme was verified with finite-element analysis and experiments.

Keywords — SRM, radial force control, sinusoidal current.

I. INTRODUCTION

The net radial force in switched reluctance motor is generally zero due to the geometrically balanced motor structure. Unbalanced radial force acting on a rotor shaft is undesirable since it causes motor vibrations. However, in the applications where the external load is not balanced, or when the rotor is not centered causing a non-uniform air gap, shaft radial force exists [1-3]. For most motors radial force can not be changed after the motor is assembled, and the force will be absorbed by the bearing and the load connected to the rotor. However, due to its special structure and the way torque is produced SRM offers a unique opportunity for controlling shaft radial force without disrupting the normal rotational torque. It is possible to produce the required radial force to cancel the forces due to non-uniform air gap or external load, and consequently motor vibrations can be reduced.

Several methods have been proposed to produce controlled radial force for SRM. A radial force and torque decoupling control scheme has been proposed for 'self-bearing' control of a 12/8 pole SRM [4-7]. In the motor each stator pole contains a main and an auxiliary winding. The main winding is used to control the motor torque. The auxiliary winding produces radial force for rotor levitation. There were a number of reports that discussed using sinusoidal current waveforms to control SRM. For example, the vector control scheme commonly used in the ac motor drives was adopted to control a three-phase SRM [8-9]. However, their objectives were mainly for torque ripple reduction and not radial force control.

Recently, a scheme which used single-phase sinusoidal excitation to control radial force of SRM was reported [10]. The main drawback of this scheme is that the maximum

attainable radial force is limited by motor torque. In particular, only small radial force can be produced when the motor is lightly loaded. Another scheme proposed to energize six poles in a 12/8 pole SRM in order to control motor torque and radial force simultaneously [11]. In this scheme, motor torque was controlled with the conventional method, i.e. all the poles in the conduction phase were excited with the same current to produce the desired torque. Two additional poles in the phase with descending-inductance were excited to produce the required radial force for rotor balancing control.

In this paper, an improved radial force control scheme based on the scheme presented in [10] for 12/8 pole SRM is proposed. The iron saturation effect was ignored; mutual inductances between stator poles are included in the analysis to improve accuracy of the model. In the conduction phase, the pole currents are energized with phase-shifted sinusoidal currents. Depending on the requested radial force and torque, the controller selects either single- or two- phase excitation. The requested force and torque are synthesized from the force and torque produced by these phases.

II. TORQUE AND RADIAL FORCE MODEL

Figure 1 shows the schematic of a 12/8-pole switched reluctance motor. Only the phase *A* windings are shown, its pole currents are designated as i_{A1} , i_{A2} , i_{A3} , and i_{A4} , respectively, and θ_r is the rotor angle in a conduction period. The aligned position is defined as $\theta_r = 0^\circ$. Because the motor stroke angle is 15 mechanical degrees ($^\circ\text{M}$), with no advancement θ_r is between -15°M to 0°M for motoring operation. Consider the attraction force produced at pole *A1*, a schematic illustrates this force is shown in Fig. 2, the magnetic flux passes through the overlapped area and the non-overlapped area due to fringing, the inductance can be modeled as

$$L_A = \frac{\mu_0 N^2 DR}{g} (\theta_o + K_{fr}) \quad (1)$$

where μ_0 is the permeability of air, K_{fr} is a constant for the fringing inductance, N is the number of turns, D is the stack length, R is the rotor radius, g is the air gap length, θ_o and θ_{uo} are the overlapped and the non-overlapped angles, respectively. θ_o and θ_{uo} are functions of θ_r . A coordinate system is attached on each stator pole to assist the attraction force analysis.

Let the amplitude and angle of the attraction force for pole *A1* be F_{A1} and θ_ϕ respectively, as shown in Fig. 2. F_{A1} is proportional to square of the pole current and varies with θ_r since L_A is a function of the rotor angle. Therefore, the

perpendicular and the parallel force component with respect to the pole $A1$ tooth can be expressed respectively as [11]

$$F_{A1_X} = K_F i_{A1}^2 \cos \theta_\phi \quad (2)$$

$$F_{A1_Y} = K_F i_{A1}^2 \sin \theta_\phi \quad (3)$$

where $K_F = L_A/4g$, and θ_ϕ can be approximated as

$$\theta_\phi = 90^\circ + \frac{\theta_{uo}}{\theta_o + K_{fr}} K_{ang} \quad (4)$$

where K_{ang} is a constant. Note that θ_{uo} is positive when the rotor is in the ascending inductance region and negative when in the descending inductance region.

Because F_{A1_X} deviates from the tangent of the rotor pole slightly, rotor torque cannot be calculated from Eq. (2) directly. Let the deviation angle be θ_p , then the torque produced by pole $A1$ can be expressed as

$$T_{A1} = -K_F i_{A1}^2 \cos(\theta_\phi + \theta_p) R \quad (5)$$

where θ_p is a non-linear function of rotor position. θ_p for the SRM used in this paper is shown in Appendix A.

When all of the poles in phase A are energized, the net radial force can be found via the vector sum of the forces produced by all poles. The amplitude and phase of the net radial force can be expressed as

$$F_r = K_F (\theta_o + K_{fr}) \cdot \sqrt{(D1 - D3)^2 + (D2 - D4)^2} \quad (6)$$

$$\theta_{fr} = \tan^{-1} \left(\frac{F_y}{F_x} \right) = \tan^{-1} \left(\frac{\sin \theta_\phi (D2 - D4) + \cos \theta_\phi (D3 - D1)}{\sin \theta_\phi (D1 - D3) + \cos \theta_\phi (D2 - D4)} \right) \quad (7)$$

where

$$D1 = i_{A1}^2 + \frac{K_{mA}}{2} i_{A1} (i_{A2} - i_{A3} + i_{A4}), D2 = i_{A2}^2 + \frac{K_{mA}}{2} i_{A2} (i_{A1} + i_{A3} - i_{A4}),$$

$$D3 = i_{A3}^2 + \frac{K_{mA}}{2} i_{A3} (-i_{A1} + i_{A2} + i_{A4}), D4 = i_{A4}^2 + \frac{K_{mA}}{2} i_{A4} (i_{A1} - i_{A2} + i_{A3}).$$

and K_{mA} is a constant of mutual inductance for phase A . Because both the self inductance and mutual inductance contribute to the radial force production, Eq.(6) contains cross-coupling terms for different pole currents. Similarly, the net motor torque can be found by summing the torque produced by each pole, and can be express as

$$T = -K_F (D1 + D2 + D3 + D4) (\theta_o + K_{fr}) \cos(\theta_\phi - \theta_p) R \quad (8)$$

It can be seen from Eqs. (6)-(8) that if the rotor angle effects are compensated for, then F_r and T can be manipulated with proper selection of $i_{A1} \sim i_{A4}$.

III. SINGLE-PHASE SINUSOIDAL EXCITATION

Let phase A be the conduction phase in the analysis. Since the polarities of the winding currents have no effect on the motor torque and radial force, it is convenient to express the sinusoidal pole currents as [10]

$$\begin{aligned} i_{A1} &= C + K \cos \theta_f \\ i_{A2} &= C + K \sin \theta_f \\ i_{A3} &= C - K \cos \theta_f \\ i_{A4} &= C - K \sin \theta_f \end{aligned} \quad (9)$$

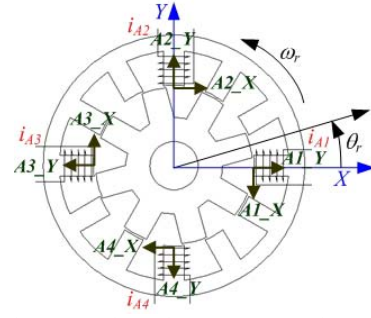


Figure 1. Schematic and coordinate systems of the 12/8 pole SRM.

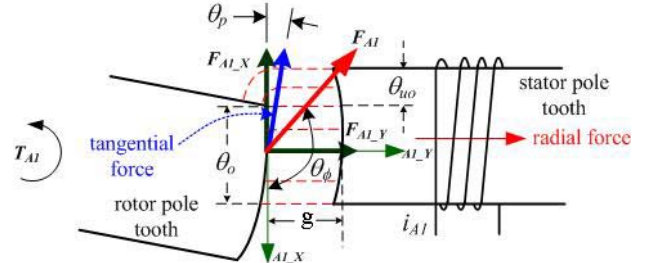


Figure 2. Attraction force produced by pole $A1$.

where θ_p , K , C are the angle, amplitude, and dc offset of the currents, respectively. These are unknowns to be determined for the desired radial force and torque. Substituting Eq. (9) into Eqs. (6)-(8), the radial force and torque become

$$F_r = 4KC \cdot K_F (\theta_o + K_{fr}) (1 + K_{mA}/2) \quad (10)$$

$$T = 4K_F (\theta_o + K_{fr}) \cos(\theta_\phi - \theta_p) R (1 + K_{mA}/2) (C^2 + K^2/2) \quad (11)$$

Rearranging the above equations such that the rotor angle dependent terms are moved to the left side, and define i_F and i_T as follows:

$$i_F^2 = \frac{F_r}{K_F (\theta_o + K_{fr}) (1 + K_{mA}/2)} = 4KC \quad (12)$$

$$\begin{aligned} i_T^2 &= \frac{T}{4K_F (\theta_o + K_{fr}) \cos(\theta_\phi - \theta_p) R (1 + K_{mA}/2)} \\ &= C^2 + K^2/2 \end{aligned} \quad (13)$$

It can be seen that F_r is a function of θ_r and is proportional to i_F^2 , therefore i_F can be considered as a *force producing current*. Also, since T is proportional to i_T^2 , i_T can be considered as a *torque producing current*. The above equations can be used to solve for the currents which produce the requested radial force and motor torque.

Let F_r^* , θ_{fr}^* , and T^* be the requested radial force, force angle, and motor torque, respectively, then from Eq.(12) the requested force producing current is

$$i_F^{*2} = \frac{F_r^*}{K_F (\theta_o + K_{fr}) (1 + K_{mA}/2)} \quad (14)$$

From Eq.(13), the requested torque producing current is

$$i_T^{*2} = \frac{T^*}{4K_F (\theta_o + K_{fr}) (1 + K_{mA}/2) \cos(\theta_\phi - \theta_p) R} \quad (15)$$

and from Eq.(7), the angle of the excitation currents is set as follows for the correct force angle,

$$\theta_f = \theta_{fr}^* - \frac{\theta_{uo}}{\theta_o + K_{fr}} K_{ang} \quad (16)$$

Equations (14)-(16) convert F_r^* , θ_{fr}^* and T^* into i_F^{*2} , i_T^{*2} and θ_f , respectively. These conversions require motor position information. Since i_F^{*2} and i_T^{*2} can also be expressed respectively as

$$i_F^{*2} = 4KC \quad (17)$$

$$i_T^{*2} = (C^2 + K^2/2) \quad (18)$$

Solving these equations simultaneously for C and K yields

$$C = \sqrt{\frac{i_T^{*2} \pm \sqrt{i_T^{*4} - (1/8)i_F^{*4}}}{2}} \quad (19)$$

$$K = \frac{i_F^{*2}}{4C} \quad (20)$$

Since K must be less than or equal to C so the resulting currents are sinusoidal, i_F is limited by

$$i_F^* \leq \sqrt{\frac{8}{3}} \cdot i_T^* \quad (21)$$

In addition to this limitation, all pole currents cannot exceed the maximum current of the motor. This limits the maximum attainable radial force. Also, Eq. (15) cannot be performed at the aligned position since the denominator is zero. Therefore, phase commutation must occur before the aligned positions.

IV. VERIFICATION WITH FINITE ELEMENT ANALYSIS

Figure 3-4 show the finite element (FE) verification of the SRM under single-phase excitation. The parameters of the SRM can be found in Appendix A. Note that the force current is limited by the maximum motor current (i_{max}), and i_T is limited by the rated torque current (i_{T_rated}). In this SRM, i_{max} and i_{T_rated} is 4.9A and 3A, respectively. i_{max} is considerably greater than i_{T_rated} so that the motor can produce radial force while delivering the rated torque.

Figure 3 shows the results when phase A is excited with $i_T = i_{T_rated}$, $i_F = i_{max}$ (pole current i also = i_{max}), and θ_f varied from 0 to 360°. This is the extreme case since the rated torque and the maximum radial force is produced. Figure 3(a)-(c) show the pole currents, motor torque, and radial force, respectively, for various θ . It can be seen that the direction of the radial force coincides with the current angle, and decrease as θ_f moves away from the aligned position. Motor torque is nearly constant regardless of θ_f and θ_r , however, no torque is produced at the aligned position. Figure 4 shows the currents and radial force when $\theta_r=0^\circ$ and $i_T=100\%$, 67%, and 33% of i_{T_rated} . It can be seen that the radial force decreased as i_T decreased. This is because the maximum i_F is limited by i_T , as shown in Eq. (21).

The shaded area in Figure 5(a) shows the allowable operating i_F vs. i_T . Since radial force and torque are functions of rotor angle, the allowable radial force and torque for a specific rotor angle can be found by substituting the currents in the shaded area of Fig. 5(a) into Eqs. (19)-(20) for C and K , and then use them and Eqs.(10)-(11) to solve for F_r and T . Figure 5(b) shows the resulting F_r vs. T for various θ . As

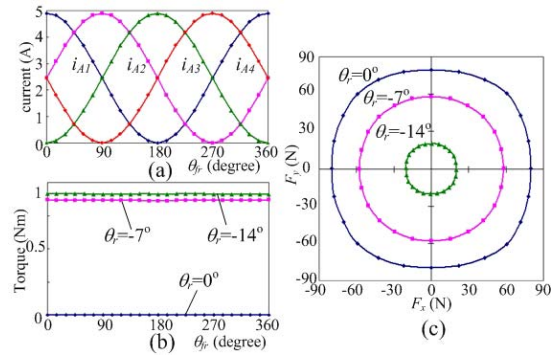


Figure 3. Radial force and torque calculated with FE under single-phase excitations, $i_T=i_{T_rated}$, $i_F=i_{max}$, θ_f varied from 0 to 360°, $\theta_r=0^\circ$, 7° , and 14° , respectively, (a) $i_{A1}\sim i_{A4}$, (b) torque, (c) radial force.

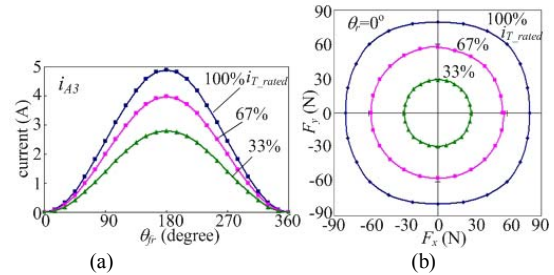


Figure 4. Radial force calculated with FE under single-phase excitations, $i_T=33\%$, 66%, and 100% i_{T_rated} , respectively, θ_f varied from 0 to 360°, $\theta_r=0^\circ$, (a) i_{A1} , (b) radial force.

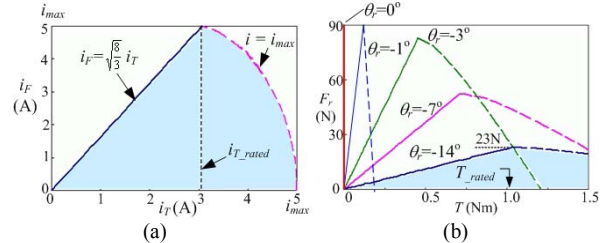


Figure 5. Operating range of the SRM under single-phase excitations for various θ_r , (a) i_F vs. i_T , (b) F_r vs. T .

shown in this figure, the operating area forms a triangle for each rotor angle. The $\theta_r=-14^\circ$ triangle is shaded for easy visualization. Notice the peaks of the triangles are the maximum force points, at these points $i_T = i_{T_rated}$ and $i_F = i_{max}$. Increase i_T beyond this point reduces the maximum available force. The maximum force increased as the rotor moved closer to the aligned position. The triangle for $\theta_r = -1^\circ$ has the largest force but the smallest torque range. The available radial force for $\theta_r = -14^\circ$ is approximately 23N as the motor delivered the rated torque.

The ability of radial force production under single-phase excitation is affected by: a) *rotor position*, a larger radial force can be produced near the aligned position, but significantly less force is available when the rotor is away from the aligned position, and b) *motor torque*, available radial force is proportional to the motor torque.

V. TWO-PHASE SINUSOIDAL EXCITATIONS

A two-phase sinusoidal excitation scheme is proposed to improve the achievable radial force. In addition to the conduction phase, in which the inductance is rising, the

descending-inductance phase is also energized. Both phases are excited with the single-phase scheme presented in the previous section. The requested radial force is supplied by the conduction and the descending-inductance phases separately. Because the descending-inductance phase produces negative torque, the conduction phase is commanded to produce the requested as well as the torque needed to cancel this negative torque.

A schematic illustrating the relationship between the force and torque produced by the energizing phases is shown in Fig. 6. In the figure, m -phase represents the conduction phase and n -phase represents the descending-inductance phase. The force and torque commands for these two phases can be expressed respectively as

$$F_m^* = (I - R_F) F_r^* \quad (22)$$

$$T_m^* = (I + R_T) T^* \quad (23)$$

$$F_n^* = R_F F_r^* \quad (24)$$

$$T_n^* = R_T T^* \quad (25)$$

where R_F and R_T are the force and torque scaling constant, respectively. Note that T_n^* is negative and the net torque is T^* . Use Eqs.(14)-(15) to convert F_r^* and T^* to the force and the torque producing currents, the above equations can be rewritten as

$$i_{Fmr}^{*2} = (I - R_F) i_{Fm}^{*2} \quad (26)$$

$$i_{Tmr}^{*2} = (I + R_T) i_{Tm}^{*2} \quad (27)$$

$$i_{Fnr}^{*2} = R_F i_{Fn}^{*2} \quad (28)$$

$$i_{Tnr}^{*2} = R_T i_{Tn}^{*2} \quad (29)$$

where i_{Fm}^* , i_{Fn}^* and i_{Tm}^* , i_{Tn}^* are the force producing currents and the torque producing currents for m - and n -phase, respectively, and the corresponding scaled currents are denoted as i_{Fmr}^* , i_{Fnr}^* , and i_{Tmr}^* , i_{Tnr}^* . Because the relative rotor position for these two phases is different, the converted i_F^* and i_T^* are also different.

As mentioned in the previous sections, i_F^* must be less than or equal to $\sqrt{8/3} i_T^*$ for valid sinusoidal currents. For convenience, i_F^* is set to $\sqrt{8/3} i_T^*$ for both phases, i.e.

$$i_{Fmr}^* = \sqrt{8/3} i_{Tmr}^* \quad (30)$$

$$i_{Fnr}^* = \sqrt{8/3} i_{Tnr}^* \quad (31)$$

Substituting these conditions into Eqs.(26)-(29), R_F and R_T can be found as

$$R_T = \frac{(3/8)(i_{Fm}^* i_{Fn}^*)^2 - (i_{Tm}^* i_{Tn}^*)^2}{(i_{Fm}^* i_{Tn}^*)^2 + (i_{Tm}^* i_{Fn}^*)^2} \quad (32)$$

$$R_F = \frac{(i_{Fm}^* i_{Tn}^*)^2 - (8/3)(i_{Tm}^* i_{Tn}^*)^2}{(i_{Fm}^* i_{Tn}^*)^2 + (i_{Tm}^* i_{Fn}^*)^2} \quad (33)$$

Once R_F and R_T are found, the scaled currents can be calculated with Eqs.(26)-(29). Then, by using Eqs.(19)-(20) the coefficients of the sinusoidal currents can be found.

Figure 7 shows the FE verification of the SRM under two-phase excitation. In this figure, the rotor position is set to -14° in phase A , torque command is 0.1Nm , and the radial force command is set to 15N , 30N , and 45N , respectively. A small torque command is used so that the requested radial force cannot be produced by phase A along. Figure 7(a) and (b) show i_{A3} and i_{B3} , respectively, (c) and (d) show the calculated torque and radial force, respectively. Note that i_{A3} and i_{B3} are not in phase since the relatively rotor angle has 15°M phase shift. It can be seen that the calculated radial forces are very accurate in spite of the rotor is near the un-aligned position and the torque is small. However, the torque has considerable errors; these errors are largely due to the modeling errors in the control scheme.

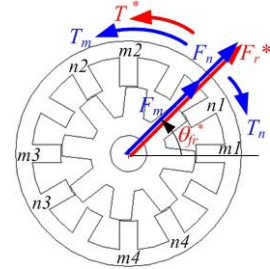


Figure 6. Force and torque for two-phase excitation.

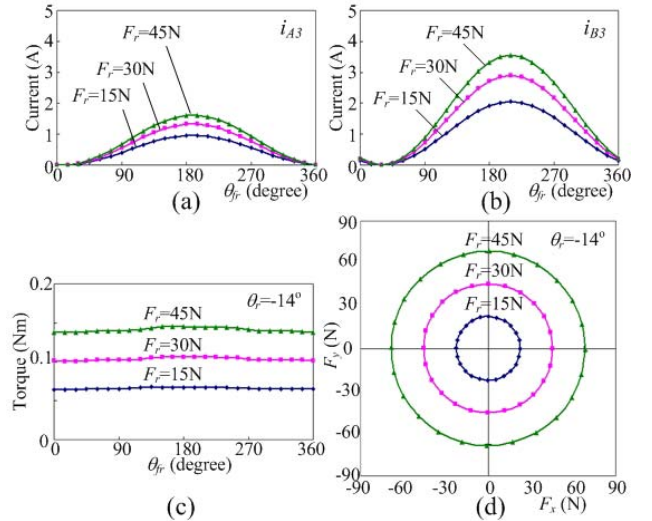


Figure 7. Radial force and torque calculated with FE under two-phase excitations, $\theta_r = -14^\circ$ in phase A , $T^* = 0.1\text{Nm}$, $F_r^* = 15\text{N}$, 30N , and 45N , respectively, (a) i_{A3} , (b) i_{B3} , (c) torque, (d) radial force.

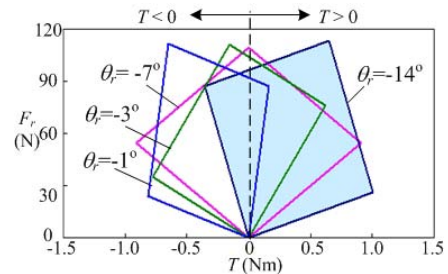


Figure 8. Operating range (F_r vs. T) of the SRM used two phase sinusoidal excitations for various θ_r .

Figure 8 shows the allowable operating range for the two-phase excitations. In the figure, F_r vs. T plot for θ_r equals -1° , -3° , -7° , and -14° , respectively, are shown. The operating area of each rotor angle forms a rectangle. Because in the two-phase excitation i_F^* is always set to $\sqrt{8/3} i_T^*$, the bottom side of each rectangle coincides with the upper side of the corresponding triangle shown in Fig.5. Excitation of the second phase enables production of significantly greater radial force when small torque is requested. Because the operating area of the two-phase excitation extends, with no overlapping, the operating area of the single-phase excitation, the two-phase scheme can be utilized only when the single-phase excitation is unable to produce the requested radial force.

VI. CONTROL SYSTEM

Figure 9 shows the block diagram of the proposed radial force control scheme. The SRM is controlled with a speed loop. Torque command T^* is generated by the motor speed controller, and F_r^* and its direction is produced by a procedure relates to the application of radial force. The flowchart shown in Figure 10 determines whether single- or two- phase excitation should be used based on the requested torque and radial force. Equations (14)-(15) and θ_r are required in this process.

After the excitation method is determined, the current commands can be calculated. Figure 11 depicts the procedures for calculating current commands for the two-phase excitation. The equations needed for the calculations are also shown in the block diagrams. Note that in the case of single-phase excitation, the calculation procedures are similar except the n -phase and the scaling are ignored.

VII. EXPERIMENTAL RESULTS

The control scheme presented in the previous sections was verified experimentally. The parameters of the SRM are shown in Appendix A. Figure 12 shows the experimental setup. The stator was placed vertically on a platform. The upper end of the rotor was connected to the housing via a universal joint and a bearing. An ac motor was mounted on top of the rotor shaft to provide load to the SRM. Four load cells were mounted on the lower end of the rotor to measure the radial force produced by the motor. The measured signals are filtered with low-pass filters. Each pole winding has its own current control loop. A DSP was used to perform all of the current, speed, and radial force controls. Hysteresis control action was used for current controllers. The current and the radial force controls were executed at 18.4 kHz, and the speed control was executed at 4.6kHz. The phase switching angle was advanced 1° in order to avoid execution of Eq. (15) at the aligned position.

Figure 13 shows the radial force and phase A currents when the SRM was at standstill and under single-phase excitations. Load torque was 1Nm, rotor position θ_r was at -14° , and the force command was set to 30N and rotating at 1Hz. It can be seen that only about 23N radial force was produced instead of 30N. This is because the motor was unable to produce the requested force when θ_r was far away from the aligned-

position with the single-phase excitation. Note that since i_T was approximately i_{T_rated} (3A) and the pole currents were at their maximum value i_{max} , the motor was operating at the peak point of the $\theta_r = -14^\circ$ triangle shown in Fig. 5(b).

Figure 14 shows the radial force, i_{A1} and i_{B1} when the SRM was at standstill and under two-phase excitation. Load torque was set to 0.1Nm, θ_r at -14° , and the force command was set to 15N, 30N, and 45N, respectively. It can be seen that with the two-phase excitation, the motor was able to produce the requested radial force even though θ_r is far away from the aligned-position and the torque is small.

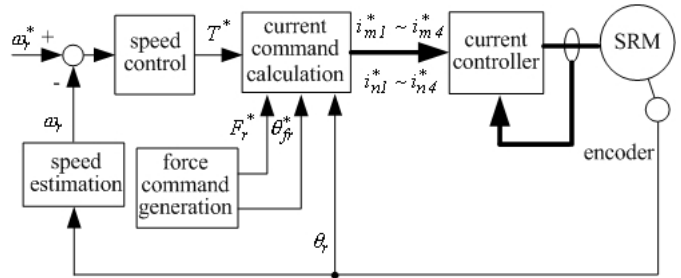


Figure 9. Radial force control system.

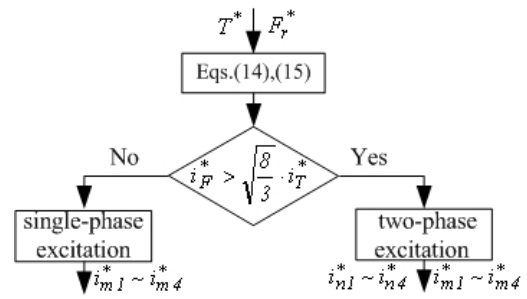


Figure 10. Selection of excitation strategy.

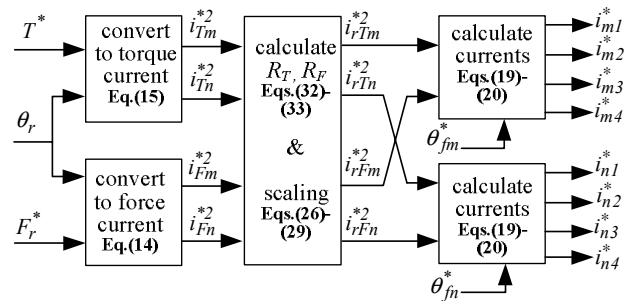


Figure 11. Calculate current commands for two-phase excitation.

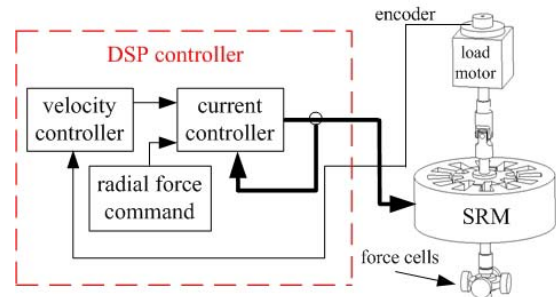


Figure 12. Experimental setup.

Figure 15 shows the radial force and phase A currents when the motor was running at 100 rpm and under 1.0Nm load torque. The force command was set to (a)0N, (b)15N, and (c)45N, respectively, and rotating synchronously with the rotor. Note that in Figs. 15(a) and (b) single-phase excitation was used since i_F^* did not exceed its limitation. However, Fig. 15(c) used two-phase excitation since i_F^* for 45N is greater than $\sqrt{8/3} i_T^*$. It can be seen that in all the cases, the measured radial force were very closed to their commanded values. The ripples in the force waveforms were caused by phase commutations, and the distortions were mainly due to the rotor eccentricity and un-symmetric structures. Figure 16 and 17 show the results when the SRM was running at the same operating conditions as that in Fig.15 except the motor speed was 500 and 1000rpm, respectively. It can be seen that the motor was able to produce the requested radial force.

Figure 18 shows (a) radial force and (b) i_{A1} current (c) speed, when the controller switched from single- to two-phase excitations. The motor was running at 500 rpm under 0.3Nm load torque. $|F_r^*|$ was set to 15N rotating synchronously with the rotor initially, and then step changed to 45N at time = 0.5sec. A small load torque was used so that the two-phase excitation was required for 45N force. It can be seen that the radial force increased to 45N smoothly. Motor speed was virtually unaffected by the step change of the radial force.

Figure 19 shows the results of varying the radial force frequency when the motor was running at 500 rpm and under 0.3Nm load torque. The radial force command was set to 45N and its frequency was set to (a)0Hz and directed toward 45° , (b)4Hz, (c)8Hz, and (d)16Hz, respectively. Note that due to large radial force demands, two-phase excitation was always used. It can be seen that the motor was able to produce the requested radial force effectively. The waveform shown in Fig.19(d) was much smoother than the other waveforms due to the filtering of the measured signal.

VIII. CONCLUSION

A 12/8-pole SRM under single-phase and two-phase sinusoidal excitations were analyzed in this paper, and a scheme to separately control radial force and motor torque was proposed. The iron saturation effect was ignored; mutual inductances between stator poles are included in the analysis to improve accuracy of the model. It is found that when the conduction phase is excited with sinusoidal currents, the SRM is capable of generating shaft radial force in any direction of the rotational plane and producing rotational torque. However, the ability of radial force production under single-phase excitation is affected by the rotor position, and is proportional to the motor torque. When the single-phase excitation can not produce the requested radial force, the phase with descending-inductance is also excited with sinusoidal currents to increase the radial force production.

The experimental results show that the SRM is able to produce controlled radial forces when the motor is at standstill or running, and subjected to a load torque. The measured radial force exhibited noticeable ripples caused by phase commutations, but the average forces were very close to the

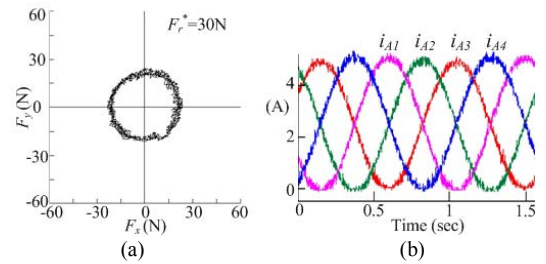


Figure 13. Radial force and phase A currents when the SRM was at standstill, $\theta_r = -14^\circ$, load torque = 1Nm, $|F_r^*| = 30\text{N}$ and rotating at 1Hz, single-phase excitation, (a) radial force, (b) pole $A1\sim A4$ currents.

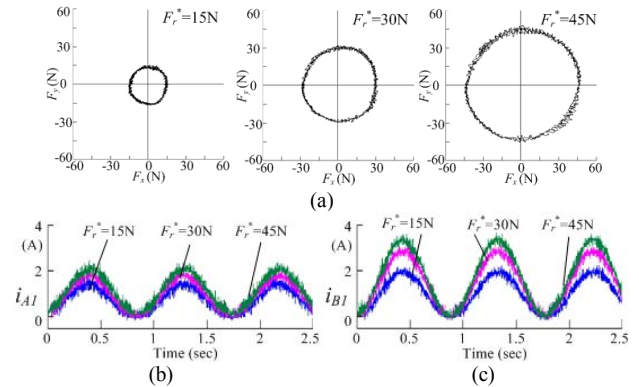


Figure 14. Radial force and phase A, B currents when the SRM was at standstill, $\theta_r = -14^\circ$, load torque = 0.1Nm, $|F_r^*| = 15\text{N}, 30\text{N}, 45\text{N}$, respectively, and rotating at 1Hz, two-phase excitation, (a) radial force, (b) i_{A1} , (c) i_{B1} .

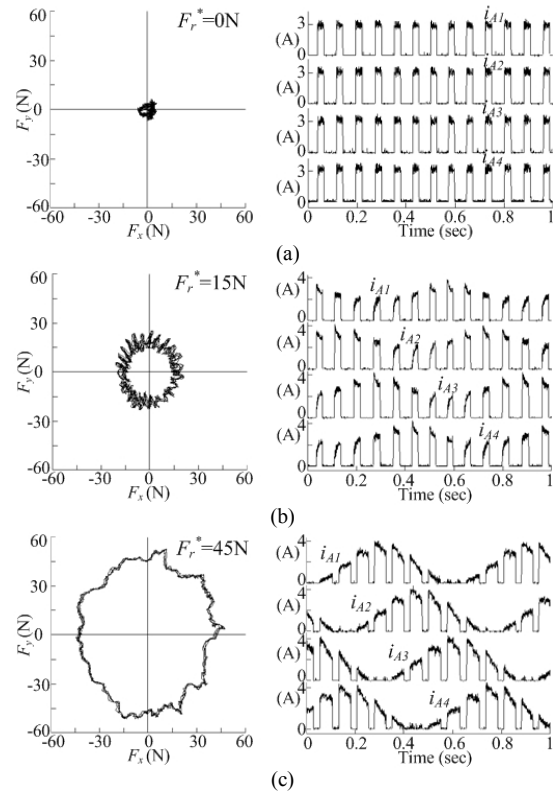


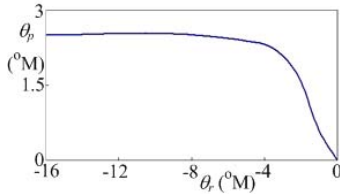
Figure 15. Radial force and phase A currents when the motor was running at 100 rpm under 1.0Nm load torque and $|F_r^*|$ set to (a) 0N, (b)15N, (c)45N, and rotating synchronously with the rotor

commanded values. Although the results shown in this paper did not include any vibration tests, the proposed scheme can be used to produce the required radial force to cancel the forces produced by a non-uniform air gap or external load, and eventually reduce motor vibrations [10].

APPENDIX A

The rating of the 12/8 pole SRM used in this paper is 100 Watts, 1000 rpm, maximum current 4.9A, its main parameters are:

Aligned inductance	8 mH
Un-aligned inductance	2 mH
K_{fr}	3.1
K_{ang}	4.1
θ_p :	



ACKNOWLEDGMENT

We gratefully acknowledge the support for this research by the National Science Council, Taiwan, R. O. C., under grant: NSC 94-2213-E-032-028.

REFERENCE

- [1] S. Ayari, M. Besbes, M. Lecrivain, and M. Gabsi, "Effects of the Air gap Eccentricity on the SRM Vibrations", International Conference on Electric Machines and Drives, 1999, pp. 138-140.
- [2] N.R. Garrigan, W. L. Soong, C. M. Stephens, A. Storage, and T.A. Lipo, "Radial Force Characteristics of a Switched Reluctance Machine", IEEE IAS Annual Meeting, Vol. 4, 1999, pp.2250-2258.
- [3] I. Husain, A. Radun, and J. Nairus, "Unbalanced Force Calculation in Switched Reluctance Machines", IEEE Trans. on Magnetics, Vol. 36, Jan. 2000, pp. 330-338.
- [4] C. Michioka, T. Sakamoto, O. Ichikawa, A. Chiba, and T. Fukao, "A Decoupling Control Method of Reluctance-Type Bearingless Motors Considering Magnetic Saturation", IEEE IAS Annual Meeting, Vol.1, Oct. 1995, pp. 405-411.
- [5] M. Takemoto, H. Suzuki, A. Chiba, T. Fukao, and M. A. Rahman, "Improved Analysis of a Bearingless Switched Reluctance Motor", IEEE Trans. on Industry Applications, Vol.37, Jan./Feb. 2001, pp. 26-34.
- [6] M. Takemoto, A. Chiba, H. Akagi, and T. Fukao, "Radial Force and Torque of a Bearingless Switched Reluctance Motor Operating in a Region of Magnetic Saturation", IEEE IAS Annual Meeting, Vol. 1, 2002, pp. 35-42.
- [7] M. Takemoto, A. Chiba, T. Fukao, "A Method of Determining the Advanced Angle of Square-Wave Currents in a Bearingless Switched Reluctance Motor", IEEE Trans. on Industry Applications, Vol. 37, Nov./Dec. 2001, pp. 1702-1709.
- [8] N.J. Nagle, and R.D. Lorenz, "Rotating Vector Method for Sensorless, Smooth Torque Control of a Switched Reluctance Motor Drive", IEEE IAS Annual Meeting, Vol.1, Oct. 1998, pp. 723-730.
- [9] T.H. Liu, Y.J. Chen, and M.T. Lin, "Vector Control and Reliability Improvement for a Switched Reluctance Motor", IEEE International Conference on Industrial Technology, Dec. 1994, pp. 538-542.
- [10] F.C. Lin and S.M. Yang, "Instantaneous Shaft Radial Force Control with Sinusoidal Excitations for Switched Reluctance Motors", IEEE IAS Annual Meeting, Seattle, Oct. 2004, pp. 424-430.
- [11] F.C. Lin, and S.M. Yang, "Modeling and Control of Radial Force in Switched Reluctance Motor", Power Electronics Specialist Conference (PESC06), Jun. 2006, Jeju, Korea.

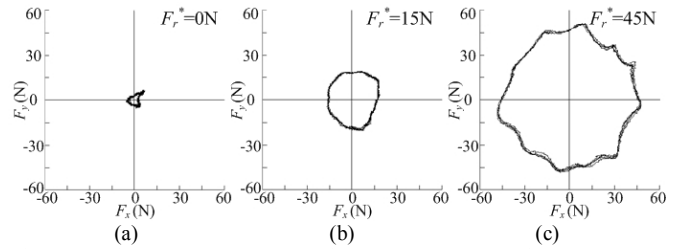


Figure 16. The SRM was running at the same operating conditions as Fig.15 except motor speed = 500rpm, $|F_r^*|$ set to (a) 0N, (b) 15N, (c) 45N

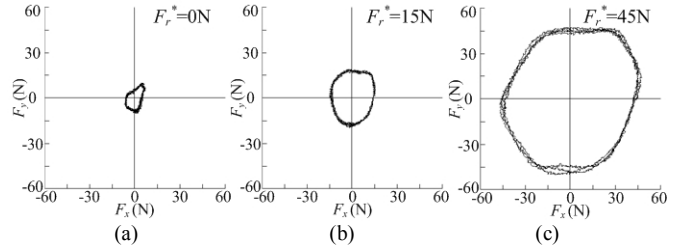


Figure 17. The SRM was running at the same operating conditions as Fig.15 except motor speed = 1000rpm, $|F_r^*|$ set to (a) 0N, (b) 15N, (c) 45N

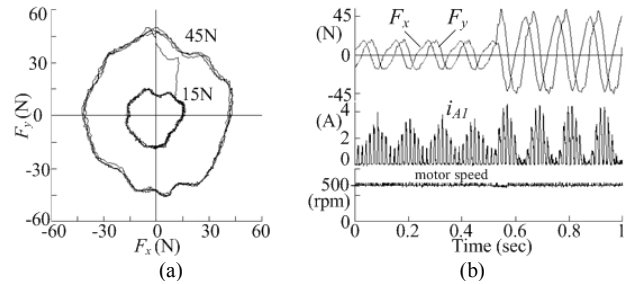


Figure 18. The SRM was running at 500rpm under 0.3Nm load torque, $|F_r^*|$ rotating synchronously with the rotor and stepped from 15N to 45N at time=0.5sec., (a) F_x vs. F_y , (b) F_x , F_y vs. time (c) i_{A1} , (d) motor speed.

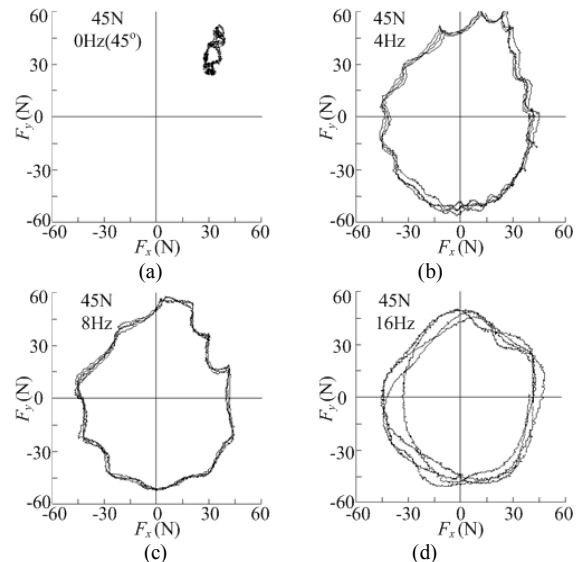


Figure 19. Radial force vector when the motor was running at 500 rpm under 0.3Nm load torque, and $|F_r^*|=45N$ and the frequency is (a) 0Hz at 45°, (b) 4Hz, (c) 8Hz, (d) 16Hz